Scanning Microscopy

Volume 1 | Number 4 Article 4

7-6-1987

An Algorithm for On-Line Digital Image Processing for Assisting Automatic Focusing and Astigmatism Correction in Electron Microscopy

Norio Baba
Kogakuin University

Eisaku Oho
Kogakuin University

Koichi Kanaya
Kogakuin University

Follow this and additional works at: https://digitalcommons.usu.edu/microscopy

Part of the Biology Commons

Recommended Citation

Baba, Norio; Oho, Eisaku; and Kanaya, Koichi (1987) "An Algorithm for On-Line Digital Image Processing for Assisting Automatic Focusing and Astigmatism Correction in Electron Microscopy," *Scanning Microscopy*: Vol. 1 : No. 4 , Article 4.
Available at: https://digitalcommons.usu.edu/microscopy/vol1/iss4/4

This Article is brought to you for free and open access by the Western Dairy Center at DigitalCommons@USU. It has been accepted for inclusion in Scanning Microscopy by an authorized administrator of DigitalCommons@USU. For more information, please contact digitalcommons@usu.edu.

Scanning Microscopy, Vol. 1, No. 4, 1987 (Pages 1507-1514)
Scanning Microscopy International, Chicago (AMF O'Hare), IL 60666 USA
0891-7035/87$3.00+.00

AN ALGORITHM FOR ON-LINE DIGITAL IMAGE PROCESSING FOR ASSISTING AUTOMATIC FOCUSING AND ASTIGMATISM CORRECTION IN ELECTRON MICROSCOPY

Norio Baba*, Eisaku Oho, and Koichi Kanaya

The Department of Electrical Engineering, Kogakuin University,
Tokyo, Japan

(Received for publication April 22, 1987, and in revised form July 06, 1987)

Abstract

An algorithm for processing a diffractogram of an electron image input by an on-line system has been improved, with the aid of projection theory, so as to achieve real time operation. This algorithm can, therefore, automatically focus in scanning electron microscope, and correct for the astigmatic aberration of both transmission and scanning electron microscopes by analyzing the spectrum computed from the diffractogram. Experimental results show that this algorithm is effective for detecting the amount of defocus and astigmatism in both transmission and scanning electron microscopes.

Keywords: On-line digital image processing, diffractogram, projection theory, automatic focusing, automatic astigmatism correction.

*Address for correspondence:
Norio Baba
Department of Electrical Engineering, Kogakuin University,
Nishishinjuku 1-24-2, Shinjuku-ku,
Tokyo, 163-91 Japan
Phone No.: 03-342-1211, ext. 274.

Introduction

Recently on-line digital image processing systems for electron microscopy are commercialized. With these on-line systems it has become possible to optimize various recording conditions for electron images by controlling a focusing lens, a stigmator and other components of an electron miscroscope (EM) provided that some improvements are accomplished (for review, see Smith 1982). Various algorithms for focusing and correcting astigmatism have been reported (see Erasmus and Smith, 1982). (Our paper does not give details of their algorithms because Erasmus and Smith (1982) have reviewed and described them in detail.) In the high resolution Transmission Electron Microscope (TEM), the optimum focusing condition in general changes according to the size of the structure being observed. In fact, the optimum focusing is not determined by a single parameter. For high resolution EM (HREM), it is therefore desirable that the focusing condition, plus other conditions such as astigmatism and resolution, be determined in real time during the observation. A diffractogram formed with phase contrast is very useful for estimating various recording conditions such as defocus, astigmatism, resolution, etc. Here, it should be noticed that for high resolution an accurate alignment of the incident illumination in the objective lens is essential. As described by Smith et al. (1983) the effect of beam misalignment is to substantially alter the phases of any diffracted electrons. When tilting the beam to show directionality in images of amorphous material, an operator would attempt to compensate for misalignment, using stigmator controls even if the phase shifts remained severe. Also in the paper (Smith et al., 1983) the contrast transfer theory for tilted illumination is formulated and described to provide a quantitative evaluation of beam tilts on high resolution imaging, and therefore the importance of beam alignment in HREM to be able to correct defocus and astigmatism must be emphasized. For the beam alignment they recommended the method using images of amorphous films recorded with the illumination successively tilted along the $\pm x$, $\pm y$ axes. In their experiment the diffractograms of the images confirmed the beam alignment (the similarity in appearance of the diffractograms indicated the alignment).

We have developed a method for analyzing the diffractogram of an electron image in order to automatically adjust the focusing and the astigmatism. The improved algorithm reported here obtains a diffractogram of a high resolution image of an amorphous

object, due to phase contrast, without invoking the two-dimensional FFT (fast Fourier transform) algorithm, thereby generating the diffractogram in real time (Baba et al. 1986). At present, the two-dimensional FFT can be done in near real-time provided that it is implemented in hardware, for example, for 256^2 pixels case in about 4 sec. Further at much higher costs, using multiple FFT processors, it is possible to reduce the time. The proposed method, however, can be performed at a higher speed without such costs and at very small memory as compared with the case of two-dimensional FFT. Using an analogue processing scheme due to Witt et al. (1972), an arbitrary section of the two-dimensional spectrum (diffractogram) is obtained by rotating the image, integrating each line of the image and calculating one-dimensional FFTs (projection theory).

In this paper the algorithm is further improved and is illustrated with some results of its application to TEM and SEM on-line images. It is also demonstrated that, by analyzing each spectrum distribution obtained by the above algorithm, changing the focusing lens excitation, and correcting the two controllers of a stigmator, automatic focusing and astigmatism correction for SEM can be realized.

On-line digital image processing system for TEM and SEM

We have assembled an on-line digital image processing system for high resolution TEM (Hitachi H-500 H, modified type; objective lens was improved, front and rear pole-piece bore radii are 4mm and 2mm, respectively, and the gap is 3mm; C_s = 0.7mm). The details are described in a previous paper (Baba et al., 1986). An image orthicon (HS-191) is coupled to a fluorescent screen by fiber plate, and this TV system is linked to a NIRECO LUZEX 5000 digital image processor. This system can process multiple images in real time. The number of images can be selected to be either 4, 8, 16, 32, 64, 128 or 256. The lowest electron dose for capturing an image by this TV system, which employs an orthicon, is 1×10^{-14} A/cm^2. The on-line computer system (LUZEX 5000) is linked to a SEM (Hitachi S-800) which can also be used as a STEM. The image from the scanning electron microscope is digitized in an analogue-to-digital converter (A-D converter) with 1024 × 1024 or 512 × 512 pixels, and the brightness of each pixel is represented by an 8-bit number, allowing 256 gray levels. At the same time, the data are stored in memory (1024 × 1024 × 8-bit 1-frame, 512 × 512 × 8-bit 10-frame equipment). The computer (CPU 68000, program memory 256kB) for image processing is linked to the image memories, and through another computer (CPU LSI-11), hard disk (10.4MB × 2), floppy disk (1MB × 2), magnetic tape, etc., are connected with the main frame. In addition to the normal recording time, we can store a series of images in a reduced recording time using a variety of A-D converter and storage systems. This is advantageous for automatic focusing and astigmatism correction at low dosages. In order to increase the speed of linear-type processing (high-emphasis filtering, averaging, gray scale transformation, geometric transformation, etc.) we employ special-purpose hardware (Oho et al., 1986).

Algorithm for obtaining central sections of a diffractogram

From the well-known equation of the Fourier transform:

$$F(q_x, q_y) = \int_{-\infty}^{\infty} \int_{-\infty}^{\infty} f(x,y)\exp\{2\pi i (x \cdot q_x + y \cdot q_y)\}dxdy \quad (1)$$

where f(x,y) represents an intensity distribution of an image, and (q_x, q_y) is the coordinate of Fourier space, the following equations are obtained:

$$F(q_x, 0) = \int_{-\infty}^{\infty} f_x \exp\{2\pi i (x \cdot q_x)\}dx, \quad (2)$$

$$f_x = \int_{-\infty}^{\infty} f(x,y)dy; \quad (3)$$

$$F(0, q_y) = \int_{-\infty}^{\infty} f_y \exp\{2\pi i (y \cdot q_y)\}dy, \quad (4)$$

$$f_y = \int_{-\infty}^{\infty} f(x,y)dx; \quad (5)$$

These equations imply that an arbitrary section of the two-dimensional spectrum (diffractogram) can be obtained by rotating the image, integrating each line of the image, and performing the one-dimensional FFT. Fig. 1 shows the flow chart for obtaining sectional profiles of the diffractogram of an on-line image. In our experiments, TEM images are input every 33msec., and SEM images every 10sec. The input image is processed on-line by masking it with a circular aperture to avoid the artifacts which tend to be exhibited when a square aperture is employed. After preprocessing, this image is rotated by an arbitrary angle to obtain an arbitrary section of the diffractogram. The gray levels of each line of the image are summed, giving a set of one-dimensional integrated image intensity values, i.e., $\{f(x_i)\ (0<i<N-1)\}$. To avoid generating artifacts, these distributions are windowed before being transformed to Fourier space. The complete two-dimensional Fourier transform is formed by appropriately combining the one-dimensional transforms. This processing is repeated for various image rotations, so that various sections of the diffractogram are obtained. In cases where the two-dimensional Fourier transform possesses homogenous frequency characteristics for radial directions, by comparing its values along various directions, the amount of astigmatism of the image can be detected within some limitations. Fig. 2 shows a test example and a confirmation of this processing. Fig. 2a is a test image of an ellipse, the longer axis of which is twice as long as the shorter axis. Fig. 2b is the diffractogram of the image (a) generated by the two-dimensional FFT algorithm. Fig. 2d shows 12-sections of the diffractogram generated by this method. Fig. 2c shows an example of the one-dimensional integrated intensity distribution of the image (a) along the x-axis. As indicated in Fig. 2d, the direction of the ellipse can be recognized. Also, when the diffractogram is regarded as an ellipse, the ratio of the lengths of the major and minor axes can be calculated as follows. If the amplitude of the diffractogram ($|F(q, \theta)|$) in a certain radial direction, identified by the angle θ, is denoted by $f\theta(q)$, and a variable $Q=nq$ is introduced, then:

$$\int_0^{\infty} f\theta(q)dq = (1/n) \cdot \int_0^{\infty} f\theta(Q)dQ. \quad (6)$$

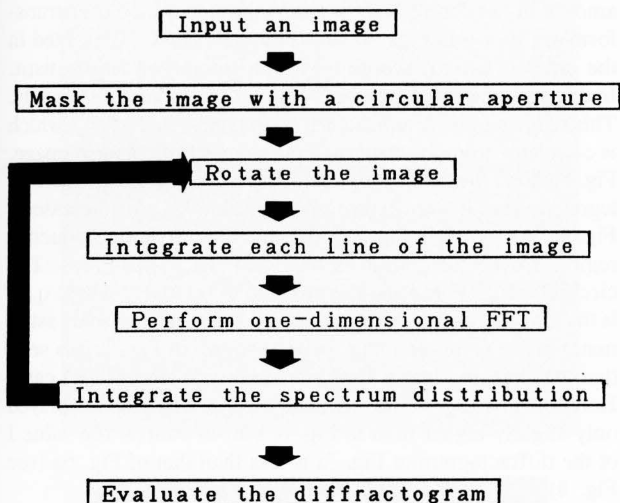

Fig. 1. Flow diagram of obtaining central sections of a diffractogram.

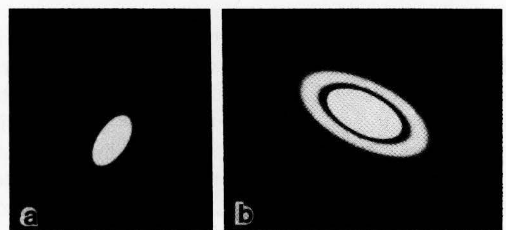

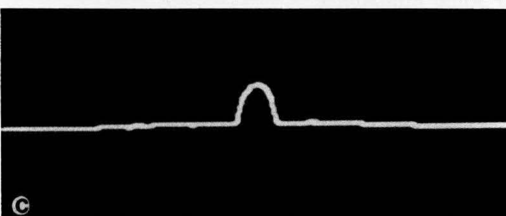

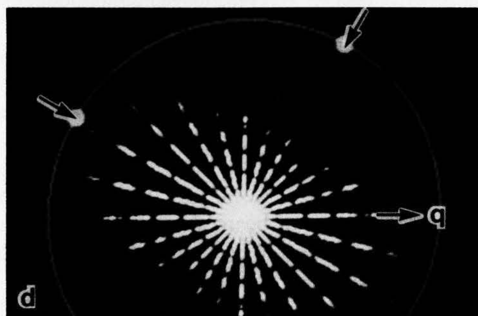

Fig. 2. A test example of a computer generated diffractogram obtained by the present projection theory; (a) an ellipse image for a test, (b) a pattern of Fourier transform of (a) generated by the two-dimensional FFT algorithm, (c) one-dimensional integrated intensity distribution of the image (a) along the x-axis; and (d) a computer generated diffractogram represented by 12-sectional profiles.

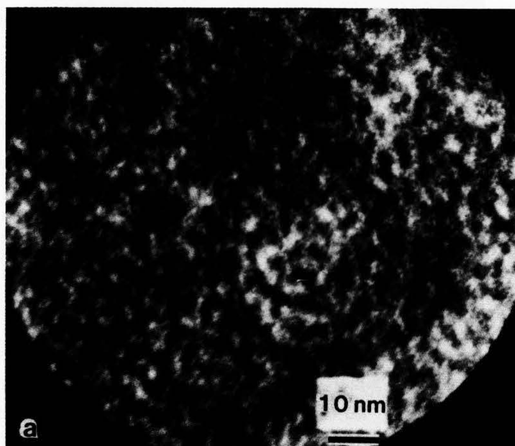

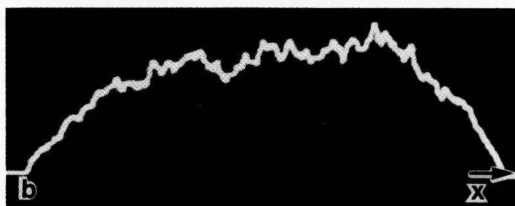

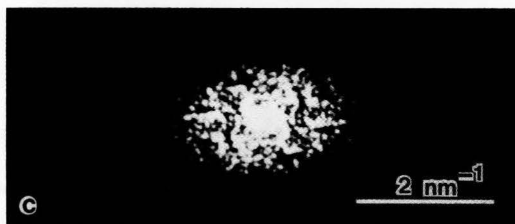

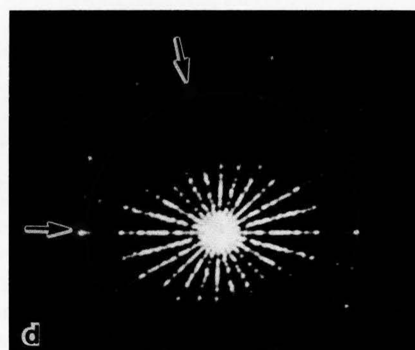

Fig. 3. An applied result of the present method to an on-line TEM image; (a) an on-line TEM image of a thin section of resin, (b) one-dimensional integrated intensity distribution of the image (a) along the x-axis, (c) a pattern of Fourier transform of (a) generated by the two-dimensional FFT algorithm; and (d) a computer generated diffractogram represented by 12-sectional profiles.

If it so happens that the image is an ellipse, so that the formula:

$$n \int_0^\infty f\theta 1\ (q)dq = \int_0^\infty f\theta 2\ (q)dq \qquad (7)$$

holds for any two directions $\theta 1$ and $\theta 2$, then the ratio is obtained from:

$$n = [\int_0^\infty f\theta 2\ (q)dq]/[\int_0^\infty f\theta 1\ (q)dq]. \qquad (8)$$

When $\theta 1$ and $\theta 2$ correspond to the directions of the minor and major axes of the ellipse, respectively, then n is the axial ratio. In our experiment, the above ratio was calculated by numerical integration. For Fig. 2d the ratio is about 2.0. Note that the arrows superimposed on Fig. 2d are in directions differing by almost 90°.

The above method is applicable to an amorphous image obtained from a high resolution TEM. Fig. 3 shows the result of applying the method to a TEM on-line image. Fig. 3a is an amorphous TEM image of a thin section of a resin input by the online system (Baba et al., 1986). Fig. 3b is the diffractogram of the image (a) generated by the two-dimensional FFT algorithm. Fig. 3d shows 12-sections of the diffractogram generated by our method. Fig. 3c shows an example of the one-dimensional integrated intensity distribution of the image (a) along the x-axis. The azimuth of the astigmatism apparent in Fig. 3d, and the ratio of about 1.6 obtained by invoking eq. (8), are probably significant in error. The latter can be reduced by independently processing several separated areas of the image.

Application to an SEM on-line system

For high resolution TEM, as described above, the azimuth of the astigmatism can in theory be estimated from only one image. However, in SEM, since the diffractogram is not homogeneous for all radial directions, it is impossible to determine the azimuth from only one image at an arbitrary setting of the controllers of the stigmator. Figs. 4 and 5 apply to SEM. Fig. 4a is an SEM image of a Pt–Pb deposition input by the on-line system and (b) is a computer generated diffractogram formed with the aid of the two-dimensional FFT algorithm. Figs. 4c and d show 24- and 12-sections of the diffractogram generated by our algorithm (see Fig. 1), which were processed much more quickly than by the general two-dimensional FFT algorithm (as shown in Fig. 4b). Fig. 5 shows another SEM example. Fig. 5a is an SEM image of latex coated balls input by the on-line system. Fig. 5b and c show 24- and 12-sections of the diffractogram generated by our new algorithm which is to be compared with computer generated diffractogram (d) processed by the two-dimensional FFT algorithm. It might seem that, from the diffraction patterns of Fig. 4c or d, the azimuth and amount of astigmatism can be determined. However, it is impossible in practice. Therefore, we need to search for the optimum setting for the two controllers in the stigmator. Our new algorithm is suitable for this purpose. Figs. 6 and 7 show the results when our new algorithm is applied to serial astigmatic SEM images altered by one controller in the stigmator. This must be regarded merely as a qualitative experimental result. Figs. 6a–d are a series of astigmatic SEM on-line images caused by a change ΔAx to one controller in the stigmator, where Ax means the total amount of the control. Six sections through the Fourier transform are shown in Figs. 6a–d. These patterns are presented in the order of a,b,c,d according to the amount of astigmatism. In this experiment the focus was preliminarily adjusted manually. This reducing rate is represented by the integrated value I which is calculated from the resulting Fourier spectrum of each image. Fig. 8 shows the normalized reducing rates, for which each integrated value I is normalized by the value I_{max} for the case of Fig. 6a. As shown in Fig. 8, it is found that when the frequency region for the integration is restricted, I/I_{max} increases. The circles on Fig. 6 indicate the position of $0.1 \cdot q_{max}$, where q_{max} is the maximum spatial frequency. Fig. 8 also applies to an astigmatic image series at under focus as shown in Fig. 7. It is seen that the changing rate is low compared with the in-focus case. Here, the intensity of the diffractograms of Fig. 7 are displayed only slightly higher than in Fig. 6, but, of course, the value I of the diffractogram of Fig. 7a is less than that of Fig. 6a (see Fig. 8).

Conclusion

An algorithm for generating arbitrary sections of the diffractogram of an electron image in real time has been described. It has been shown that the algorithm is effective for assisting automatic focusing and astigmatism correction systems which rely on detecting changes in diffractograms. Our experiments in TEM and SEM on-line systems have shown that integrated values (within a properly restricted frequency region) through several sections of the diffractograms of input astigmatic images are appropriately changed according to the amount of astigmatism. Our results indicate that our method is useful for automatic focusing and astigmatism-correction of an electron microscope under some limitations.

References

Baba N, Oho E, Mukai M, Kanaya K. (1986). Digital image processing for nonperiodic objects and an on-line image processing system for high resolution electron microscopy. J. Electron Microsc. Technique. **4**, 55–62.

Erasmus SJ, Smith KCA. (1982). An automatic focusing and astigmatism correction system for the SEM and CTEM. J. Microsc. **127**, 185–199.

Oho E, Kobayashi M, Sasaki T, Adachi K, Kanaya K. (1986). Automatic measurement of scanning beam diameter using an on-line digital computer. J. Electron Microsc. Technique. **3**, 159–167.

Smith DJ, Saxton WO, O'Keefe MA, Wood GJ, Stobbs WM. (1983). The importance of beam alignment and crystal tilt in high resolution electron microscopy. Ultramicroscopy **11**, 263–282.

Smith KCA. (1982). On-line digital image processing. Proceedings of the 10th International Congress on Electron Microscopy, Hamburg, the Deutsche Gesellschaft für Elektronenmikroskopie e. V., Vol. 1, 123–130.

Witt V, Engelmeier HP, Hoppe W. (1972). Fourier analysis of the image in the electron microscope. In: Electron Microscopy 1972. Institute of Physics, London and Bristol, 632–633.

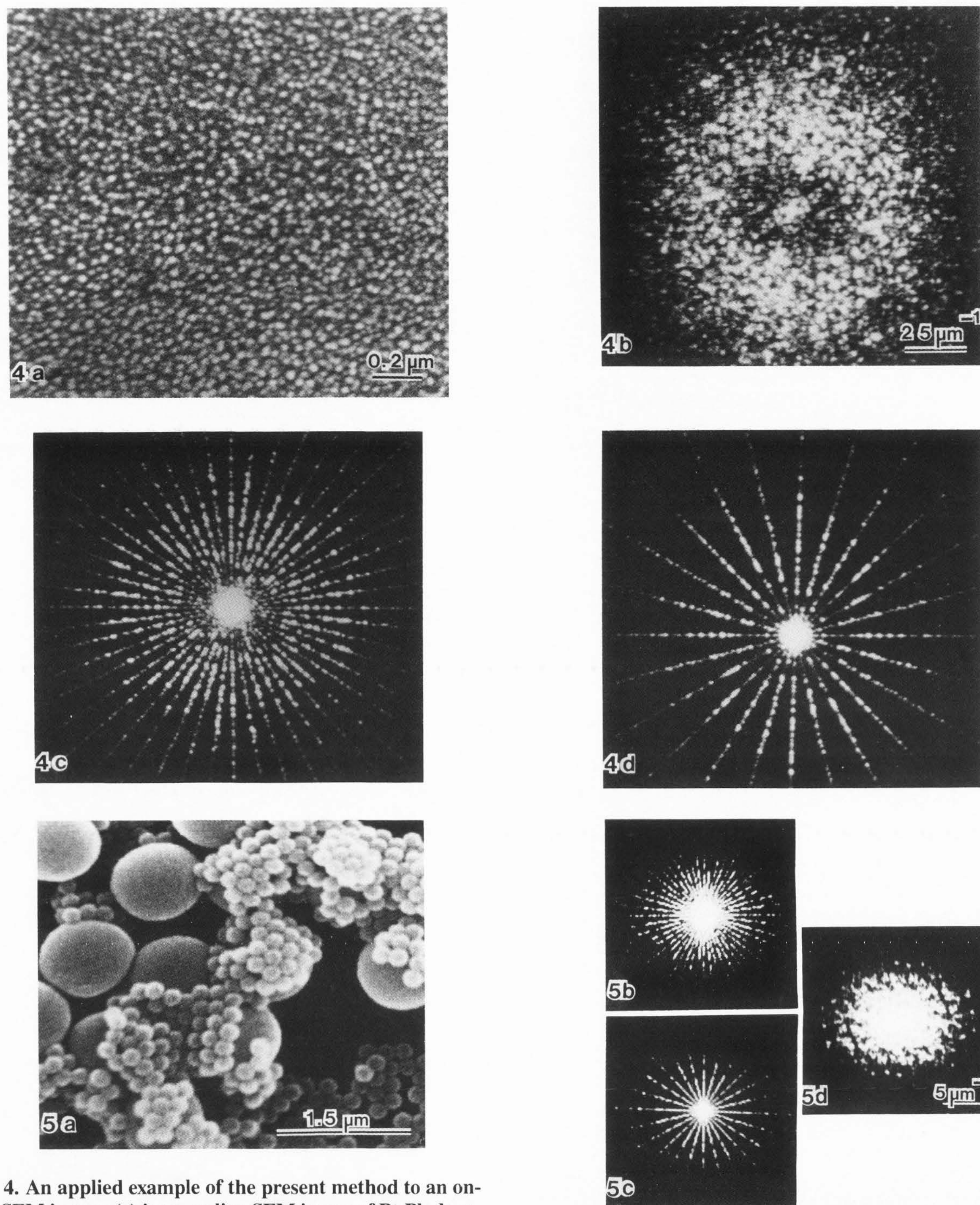

Fig. 4. An applied example of the present method to an on-line SEM image; (a) is an on-line SEM image of Pt-Pb deposited specimen, (b) a pattern of Fourier transform of (a) generated by the two-dimensional FFT algorithm, and (c) and (d) computer generated diffractograms represented by 24 and 12-sectional profiles, respectively.

Fig. 5. An applied example of the present method to an on-line SEM image; (a) an on-line SEM image of latex balls coated, (b) and (c) computer generated diffractograms represented by 24 and 12-sectional profiles, respectively; and (d) a pattern of Fourier transform of (a) generated by the two-dimensional FFT algorithm.

Discussion with Reviewers

W.O. Saxton: If the image is actually rotated after digitization, how is this done? (The process is very slow in most image processing systems).

Authors: The rotation of the image, in practice, is performed with an "address generator" for the image memory. As rotation angles can be fixed the "address generator" is not made in software but can be made in hardware. Therefore it is conceivable

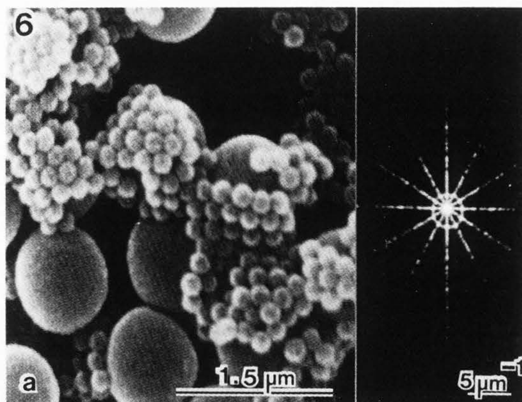
6
a
1.5 μm
5μm⁻¹

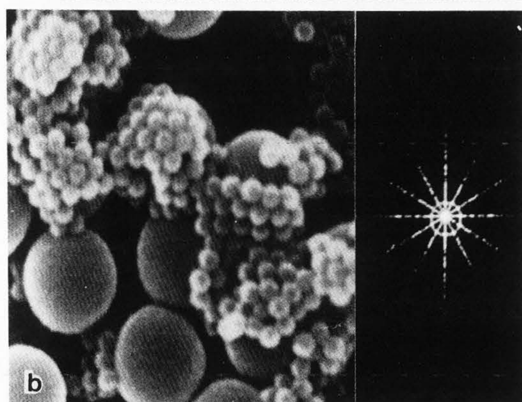
b

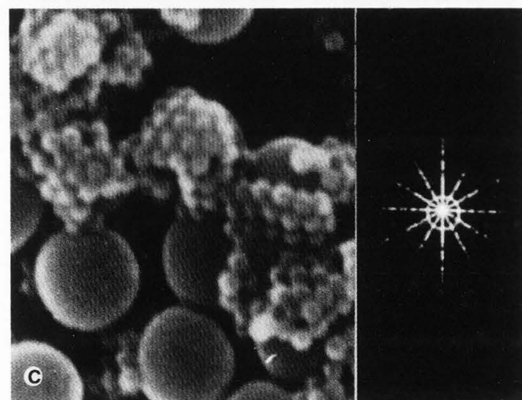
c

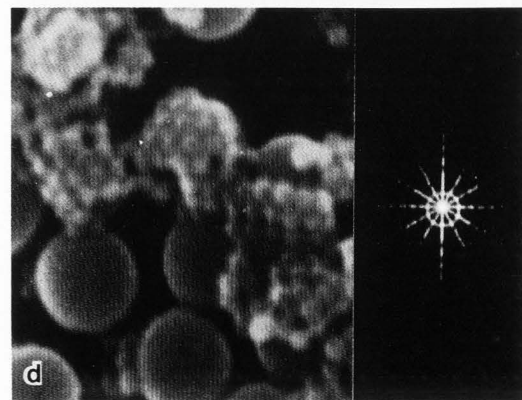
d

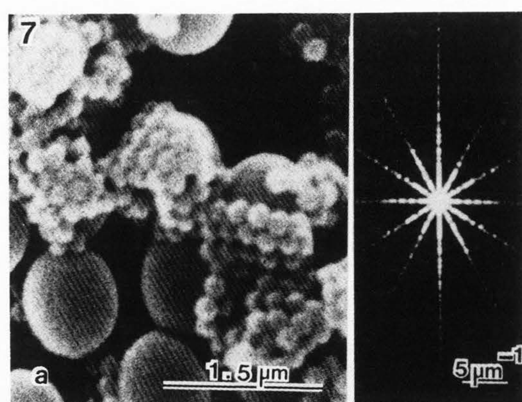
7
a
1.5 μm
5μm⁻¹

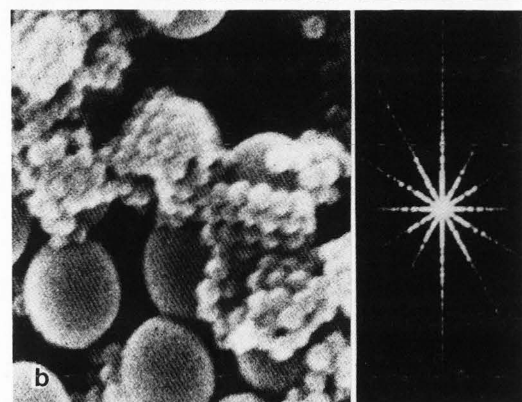
b

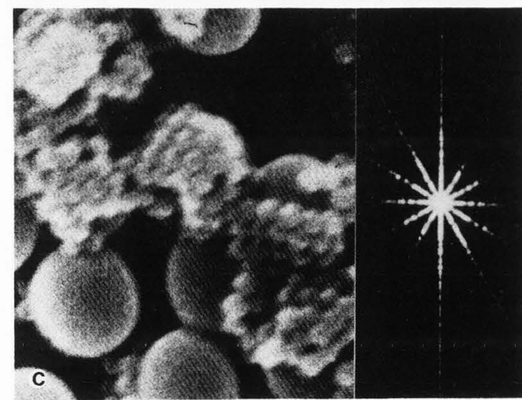
c

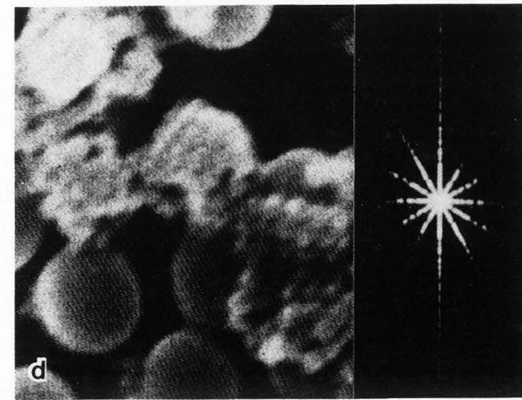
d

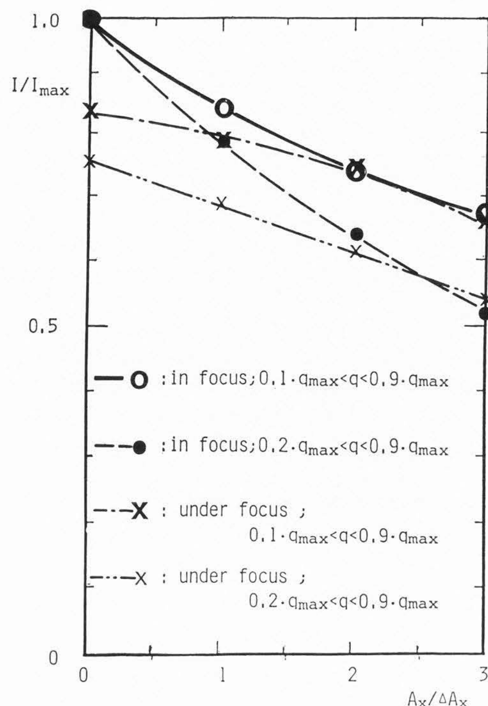

Fig. 8. Detecting effect of astigmatism by the present method when used I/I_{max} values for serial astigmatic images, where I is an integrated value of the resulting Fourier spectrum distributions for 6 directions.

that the rotation is included in the line-integration process, namely, the line-integration is executed by hardware consisting of "address generator" plus "adder". Then, it is estimted that the practical processing time roughly depends on the time for the adding which is about 300nsec./pixel (considering, of course, the rotation case). Accordingly, for 256 × 256 pixels it is expected that our algorithm for 6- and 12-directions are performed in about 0.12sec. and 0.24sec (~ 12×256×256×300nsec), respectively.

W.O. Saxton: Does Fig. 8 refer to Fig. 7 or to Fig. 6? The text asserts both, which cannot be true. Please explain.

Authors: Due to poor preservation conditions of the photographic films Figs. 7a–d had become noisy as compared to Figs. 6a–d. Also, as described in the text the intensity in display of the diffractogram series of Fig. 7 was slightly higher than in Fig. 6. This might cause a misconception. The values of I/I_{max} for 4 diffractograms in the series shown in Fig. 6(a–d) are plotted in Fig. 8 with ○ and ●, and for the 4 diffractograms shown in Fig. 7 (a–d) with **X** and X. ○ and **X** are results calculated by integrating the Fourier spectrum in six sections between $0.1 \cdot q_{max} < q < 0.9 \cdot q_{max}$ ($0.1 \cdot q_{max}$ is indicated with a circle in the diffractogram series in Fig. 6), and ● and X are for between $0.2 \cdot q_{max} < q < 0.9 \cdot q_{max}$.

The series in Fig. 6 is for the case of in-focus setting, and therefore, even when the stigmator controller is changed, the change of images or diffractograms is similar to the case of defocus change. As compared with this, the Fig. 7 series is for the case that first the focus is deviated from the in-focus position (to under focus), namely, the SEM image changes from Fig. 6a to Fig. 7a and secondly one stigmator controller is changed in series. Therefore, a directionality appears in the images and diffractograms (see especially Fig. 7d). Since the cases of Figs. 6 and 7 are considered as typical cases (the changing rate, I/Imax, of the defocus case Fig. 7 is low compared with the in-focus case Fig. 6), we have included both results.

W.O. Saxton: 2-D FFT can be done in near real-time; 256^2 in 4s already offered commercially; 512^2 in 0.5s about to be released. The problem is cost rather than feasibility. Please comment.

A.J. Koster: For comparison: how much time (or how many calculations) does it take to calculate a 2-D FFT compared to rotate the images, integrate the lines and perform the 1-D FFTs? How fast are boards for a 2-D FFT suitable for a PC?

Authors: Our method is performed by repeating the process consisting of almost 3 steps, rotating the image, integrating each line of the image and calculating 1-D FFT. The processing time is dominated by that of the integration because 1-D FFT can be done in about 1 or 2msec with hardware that is negligible and the rotation of the image, in practice, is performed with an "address generator" for the image memory in hardware (rotation angles are fixed) and therefore included in the line-integration process. As argued above, our algorithms could be performed in 0.12 or 0.24 sec, respectively. Compared to this, at present, the processing time of commercially offered 2-D FFT which is made in hardware, is about 4 sec as pointed out by the reviewer.

The cost of our processing and that of 2-D FFT seems to be nearly the same except for memory because the same FFT processor can be used. However, relatively more memory is necessary in 2-D FFT [for example, 256 × 256 × 32 bit × 2, (2 means real and imaginary parts) compared with our processing (256 × 1 × 16 bit × 2)]. If multiple FFT processors, at much higher cost (maybe more than 10 times), are used, the 2-D FFT can be done in a very short time, for example, 512 × 512 in 0.5 sec as pointed out by the reviewer. However, the above-mentioned time, 300nsec./pixel for adding can be shortened to 100nsec. by using high-speed memories and devices. Furthermore, by using multiple "address generators" and "adders" (at much lower cost than that for multiple FFT processors) the total time for our processing can even be reduced to considerably less than the time for a high cost 2-D FFT processor.

W.O. Saxton: It seems that the major/minor axis ratio can only be determined from equation (8) after the directions θ_1, θ_2 of these axes have been determined visually. If this visual step is necessary, the process cannot be described as automatic.

Moreover, an automatic procedure must also interpret the ellipticity in terms of stigmator current changes; that too is quite difficult. Please comment.

Fig. 6. An astigmatic SEM image series in the order of (a), (b), (c) and (d) together with their diffractograms represented by 6-sectional profiles, where the focus is adjusted and one controller of the stigmator is changed in series.

Fig. 7. An astigmatic SEM image series in the order of (a), (b), (c) and (d) together with their diffractograms represented by 6-sectional profiles for the defocus case where one controller of the stigmator is changed in series similarly to Fig. 6.

Authors: As you pointed out, in general, it is difficult to interpret the ellipticity of the diffractogram. Hence, in this stage, this simple evaluation manner is restricted for the defocus range. This method is not suitable for over focus region including in-focus with a very large amount of astigmatism because the diffractogram might be no longer an ellipse or eq. (7) cannot be used. (In this case it is necessary to move to enough under-focus region in the manual mode and automatically correct the astigmatism and, after this, return to first focus position. At this stage we do not think about automatic defocus correction for TEM but about automatic astigmatism correction.) This simple method can evaluate the ellipse with certain accuracy (can detect the directionality) for the under focus region from the Scherzer focus if a diffractogram at Scherzer focus cannot be interpreted as an ellipse because of the very large amount of astigmatism, of course, the method cannot be used). If a diffractogram obtained is within the above limitation, comparing integrated values of the spectrum in radial direction to each other the direction for the maximum value or the direction for the minimum value is regarded as the major or minor axis, respectively.

W.O. Saxton: The noisy, highly speckled character of TEM diffractograms means that a ring pattern may well not be obvious in a few sections such as the one calculated. Fig. 3 seems to me to illustrate this problem clearly. Please comment.
Authors: As described above, in this stage, this method is suitable for under focus region from the Scherzer focus. As pointed out by you the ring pattern may well not be obvious in a few sections. However, within the above limitation, the present method can catch the difference of radial spectrum distributions due to the ellipticity because the effect of integration of spectrum in a direction may be regarded as a statistical effect to the noisy character of TEM diffractograms. Of course, to reduce the error, independent processing of several separated areas of the image is necessary.

A.J. Koster: How accurate is the estimate for the power spectrum of the image using (or without) a window? What is the influence of a poorly estimated power spectrum on the accuracy of defocus and astigmatism measurement? Up to which spatial frequencies do you expect to use the power spectrum estimate? What are the limitations of the method?
Authors: In the present method a problem that causes a lack of accuracy is a rotation of an image because the rotation is, in fact, achieved by digital (not analog) processing. Therefore, there are errors in vicinity of the highest frequency regions in the Fourier spectrum distribution. However, if one records an image at sufficient magnification taking this error into consideration, in practice the error can be neglected. In this experiment a window was used to eliminate an artifact arising from differences of image area for rotations due to lack of image data because the image data before rotation is square.

At the present, in the case of TEM we plan to automatically correct mainly astigmatism (we do not think about automatic defocus correction for TEM now), and in the case of SEM we plan to automatically correct both defocus and astigmatism. For automatic processing, more simple algorithm is desired. For TEM our method described in the text (see Eq. 7) is a simple method for evaluating an ellipse of a diffractogram, but as pointed out by the reviewer the method may not be accurate and cannot measure the amount of astigmatism accurately in this stage. However, this simple method can evaluate the ellipse with reasonable accuracy (can detect the directionality) for the under-focus region from the Scherzer focus. As mentioned above, at present, we do not plan for automatic defocus correction for TEM but only for automatic astigmatism correction. First the equations of spatial frequencies for a weak phase object were considered, and as a result it was conceivable that in the case of over-focus regions, including in-focus with very large amounts of astigmatism, this method was frequently unsuitable because the diffractogram might no longer be an ellipse and Eq. (7) could no longer be used.

For SEM, since integrated values (within a properly restricted frequency region) through several sections of the diffractograms of input defocus or astigmatic images are appropriately changed according to the amount of defocus or astigmatism, an automatic focusing and astigmatism correction can be realized.